The Zinc Transporter ZnT3 Interacts with AP-3 and It Is Preferentially Targeted to a Distinct Synaptic Vesicle Subpopulation

Gloria Salazar, *Emory University*
Rachal Love, *Emory University*
Erica Werner, *Emory University*
Michele M. Doucette, *Emory University*
Su Cheng, *Emory University*
Allan I Levey, *Emory University*
Victor Faundez, *Emory University*

Final published version: http://www.molbiolcell.org/content/15/2/575

Copyright information:

The Zinc Transporter ZnT3 Interacts with AP-3 and It Is Preferentially Targeted to a Distinct Synaptic Vesicle Subpopulation

Gloria Salazar,* Rachal Love,* Erica Werner,* Michele M. Doucette,* Su Cheng,* Allan Levey,[†#] and Victor Faundez*[‡#]

*Departments of Cell Biology and [†]Neurology, and [#]The Center for Neurodegenerative Diseases, Emory University, Atlanta, Georgia 30322

Synaptic vesicles (SV) are generated by two different mechanisms, one AP-2 dependent and one AP-3 dependent. It has been uncertain, however, whether these mechanisms generate SV that differ in molecular composition. We explored this hypothesis by analyzing the targeting of ZnT3 and synaptophysin both to PC12 synaptic-like microvesicles (SLMV) as well as SV isolated from wild-type and AP-3–deficient *mocha* brains. ZnT3 cytosolic tail interacted selectively with AP-3 in cell-free assays. Accordingly, pharmacological disruption of either AP-2- or AP-3–dependent SLMV biogenesis preferentially reduced synaptophysin or ZnT3 targeting, respectively; suggesting that these antigens were concentrated in different vesicles. As predicted, immuno-isolated SLMV revealed that ZnT3 and synaptophysin were enriched in different vesicle populations. Likewise, morphological and biochemical analyses in hippocampal neurons indicated that these two antigens were also present in distinct but overlapping domains. ZnT3 SV content was reduced in AP-3–deficient neurons, but synaptophysin was not altered in the AP-3 null background. Our evidence indicates that neuroendocrine cells assemble molecularly heterogeneous SV and suggests that this diversity could contribute to the functional variety of synapses.

INTRODUCTION

The molecular diversity in total brain synaptic vesicle (SV) composition is generally presumed to result from differential expression of synaptic vesicle membrane proteins in different brain regions. However, the possibility that synaptic vesicles differ in composition because of different biogenesis mechanisms has not been explored. Different vesiculation pathways could result in molecularly diverse synaptic vesicles. Vesiculation mechanisms are known to produce distinct cargo carriers from a population of donor membranes (Bonifacino and Dell'Angelica, 1999; Springer *et al.*, 1999; Boehm and Bonifacino, 2001). This process is achieved by adaptor complexes that recognize and concentrate specific membrane proteins in the donor membranes (Bonifacino and Dell'Angelica, 1999; Kirchhausen, 1999). PC12 cells have been shown to possess two such adaptor-dependent pathways for the assembly of synaptic vesicles, also known as synaptic-like microvesicles (SLMV) (Shi *et al.*, 1998; de Wit *et al.*, 1999; Jarousse and Kelly, 2001). In one pathway, SLMV are generated from the plasma membrane by a vesiculation mechanism that requires the adaptor AP-2, clathrin, and the GTPase dynamin (Shi *et al.*, 1998). In the second pathway, SLMV are generated from endosomes by the adaptor complex AP-3 (Faundez *et al.*, 1998; Blumstein *et al.*, 2001) and the GTPase ARF1 (Faundez *et al.*, 1997). In contrast to the plasma membrane pathway, the endosome-

derived mechanism is highly sensitive to brefeldin A (BFA) (Shi *et al.*, 1998).

Phenotypes observed in the AP-3–deficient *mocha* mouse are consistent with a role for the AP-3–dependent, endosome-derived pathway in neurons (Kantheti *et al.*, 1998). The *mocha* mossy fibers are devoid of both the synaptic vesicle-specific zinc transporter ZnT3 and vesicular ionic zinc (Palmiter *et al.*, 1996; Kantheti *et al.*, 1998). Synaptic terminals from this mouse possess an overall normal morphology (Kantheti *et al.*, 1998), suggesting that the synaptic phenotype of this mutation is due to deficiency in a subpopulation of SV that contain the zinc transporter or in the targeting of a discrete set of SV proteins, rather than a generalized synaptic vesicle defect.

Although two different adaptors can generate SLMV from distinct subcellular locations in PC12 cells, it is presently unknown whether these vesicles differ in composition. We tested this hypothesis using the zinc transporter 3 protein (ZnT3) and synaptophysin as SV reporters. We found that the AP-3 complex preferentially recognizes ZnT3 compared with synaptophysin both in vitro and in vivo. Biochemical evidence suggests that ZnT3 and synaptophysin are enriched in different synaptic or synaptic-like vesicle populations. Consistent with these data, simultaneous staining with both zinc- and pH-sensitive dyes in living cells indicates that secretory compartments with heterogeneous contents are present in boutons of cultured hippocampal neurons. Together, these results support the hypothesis that neuroendocrine cells assemble synaptic vesicles that differ in their composition. These findings have important implications for understanding how diversity in neuronal signaling might be generated at the synapse.

MATERIALS AND METHODS

Cell Culture and Transfection

PC12 KB, PC12 VAMP II N49A, and PC12 Vglut1 cells were maintained as described previously (Grote *et al.*, 1995). Human embryonic kidney (HEK)293 cells were grown on DMEM medium (Cellgro) (4.5 g/l glucose), supplemented with 10% fetal calf serum (Hyclone Laboratories, Logan, UT) and 100 U/ml penicillin and 100 μg/ml streptomycin (Cellgro). Transfections were performed with Effectene (QIAGEN, Valenica, CA) following manufacturer protocols. Permanently transfected cells were selected in 0.8 mg/ml G418 and maintained in 0.25 mg/ml G418. Expression was induced by 6 mM sodium butyrate for 12–24 h, as described previously (Grote *et al.*, 1995).

Primary cultures of hippocampal neurons were performed as described previously (Craven *et al.*, 1999). Briefly, hippocampi from 1- to 4-day postnatal rats were enzymatically digested and plated onto either 10-mm #0 MatTek dishes or 15-mm #0 Deckglaser German glass coverslips coated with Matrigel. Cells were cultured in neurobasal medium supplemented with B27 supplement, L-glutamine, and penicillin/streptomycin plus 8 μM AraC. Cells were used after 6–14 d in vitro (DIV).

Antibodies, Plasmids, and Recombinant Proteins

Antibodies used in this study were monoclonals anti-synaptophysin (SY38; Chemicon International, Temecula, CA), VAMP II (69.1; Sysy; Goettingen, Germany), SV2 (10H4; a gift of Dr. R. Kelly; University of California, San Francisco, CA), anti-transferrin receptor (H68.4; Zymed Laboratories, South San Francisco, CA), anti-green fluorescent protein (GFP) (11E5; Molecular Probes, Eugene, OR), anti-hemagglutinin (HA) (12CA5; a gift from Dr. Y. Altschuler; Hebrew University, Jerusalem, Israel), anti-KDEL receptor (Stressgen; San Diego, CA), anti-rabaptin 5 and TGN38 (BD Transduction Laboratories, Lexington, KY), anti-myc and anti-LAMP II (9E10 and H4C5; Developmental Studies Hybridoma Bank, University of Iowa, Iowa City, IA). Anti anti-vesicular glutamate transporter (Vglut1) and vacuolar ATPase antibodies were obtained from Sysy, and chloride channel 3 (ClC3) was a gift from Dr. D.J. Nelson (University of Chicago, Chicago, IL). All AP-3 antibodies have been described previously (Salem *et al.*, 1998; Faundez and Kelly, 2000). Polyclonal antibodies against a glutathione *S*-transferase (GST) fusion protein encompassing ZnT3 residues 1–78 were made in rabbits (Alpha Diagnostic International) and affinity purified as described previously (Roos and Kelly, 1998).

ZnT3 cDNA, a generous gift of Dr. R. Palmiter (University of Washington, Seattle, WA), was subcloned either in pEGFPN1 or pcDNA 3.1. A single HA epitope was introduced to the ZnT3 carboxy terminus by polymerase chain reaction (PCR) by using pcDNA3.1-ZnT3. β3B (a gift of Dr. R. B. Darnell; the Rockefeller University, New York, NY) and μ3b cDNAs (a gift of Dr. R. Scheller; Genentech; South San Francisco, CA) were amplified by PCR with primers encoding unique restriction sites and subcloned in frame in the vector pcDNA 3.1 Myc-His +A.

The residues 1–78 of ZnT3 were PCR amplified using the ZnT3 cDNA as a template, whereas the whole carboxy-terminal tail (residues 285–388) was amplified from mouse brain Quick Clone cDNAs (BD Biosciences Clontech, Palo Alto, CA). Both inserts were cloned into pGEX-5×-1 by using *Eco*RI and *Xho*I sites. The GST fusion protein encoding the carboxy terminal tail of synaptophysin was a generous gift of Drs. C. Daly and E. Ziff (New York University, New York, NY). Recombinant proteins were generated as described previously (Roos and Kelly, 1998), concentrated and dialyzed against intracellular buffer. All PCR reactions were performed with high-fidelity Pfu polymerase and products cloned in TOPO cloning vectors. Both strands of all the constructs were sequenced.

Immunolocalizations

Cells were washed in phosphate-buffered saline (PBS) with Ca/Mg containing 10 mM glucose and perforated with 0.02% saponin in Dulbecco's PBS (DPBS) with Ca/Mg for 5 min at 4°C. After washing, cells were fixed for 20 min at 4°C in 4% paraformaldehyde and processed for immunofluorescence as described previously (Faundez *et al.*, 1997; Wei *et al.*, 1998). Secondary antibodies used were Alexa-conjugated goat anti-mouse 488 and/or goat anti-rabbit 568.

Confocal Microscopy/Two-Photon Microscopy

To image zinc-containing compartments, cells were loaded with 25 μM ZnSO$_4$ in calcium/magnesium-free Hanks' balanced salt solution containing 10 mM Na-pyruvate, 10 mM glucose, penicillin/streptomycin for 1 h at 37°C. Free zinc was washed at 4°C, and cells were loaded with 25 μM zinquin and/or 1 μM Lysosensor Green-DND 189 in 10 mM glucose DPBS for 30 min at 37°C. Excess dye was extensively washed at 4°C, and cells were kept at 4°C until imaged at 22°C except when cells were incubated with α-latrotoxin (10 nM; Alomone Labs, Jerusalem, Israel). Neurons or GFP-PC12 cells were imaged at 37°C on MatTek dishes warmed with a Bioptechs objective heating system. A single image was taken before the addition of the drug or toxin. Times series were taken from each dish with 15.7-s intervals between slices for neurons and every 201.6 s for GFP-transfected PC12 cells.

Specimens were viewed using an Axiovert 100M microscope (Carl Zeiss, Thornwood, NY) coupled to a HeNe1, Argon ion and a Coherent Verdi pumped Ti:Saphire laser. Zinquin was excited with the Ti:Saphire laser tuned at 750 nm. Images were acquired using LSM 510 sp1 software (Carl Zeiss). Emission filters used for acquisition from live imaging experiments were LP505 and BP465 IR. The emission filters used for immunofluorescence were LP505 and BP 500-550 IR. All images were viewed and acquired using a Plan Apochromat 63×/1.4 oil DiC objective.

Images were processed and analyzed using MetaMorph software, version 3.0 (Universal Imaging, Downingtown, PA). All individual images had separate threshold values set. Three or four regions of interested were used for each individual image for colocalization values.

Cell Fractionation and Synaptic Vesicle Purification

Cells were homogenized in intracellular buffer (38 mM potassium aspartate, 38 mM potassium glutamate, 38 mM potassium gluconate, 20 mM MOPS-KOH, pH 7.2, 5 mM reduced glutathione, 5 mM sodium carbonate, 2.5 mM magnesium sulfate, 2 mM EGTA) by using a cell cracker with a 12-μm clearance according to Clift-O'Grady *et al.* (1998). The homogenate was sedimented for 5 min at 1000 × *g* to obtain a S1 supernatant. S1 fractions were sedimented at 27,000 × *g* for 35 min to generate S2 supernatants. S2 were spun either at 210,000 × *g* for 1 h in a Beckman Coulter TLA120.2 rotor (P3) or through glycerol velocity gradients (5–25%) prepared in intracellular buffer at 218,000 × *g* for 75 min in a SW55 rotor (Beckman Coulter, Fullerton, CA). Alternatively, PC12 cell homogenates were spun in sucrose velocity gradients as described previously (Lichtenstein *et al.*, 1998). The SV peak was determined by immunoblot with antibodies against ZnT3, VAMP II, and synaptophysin. Rat brain SV were isolated according to Clift-O'Grady *et al.* (1990). All procedures were performed at 4°C in the presence of the antiprotease mixture Complete (Roche Molecular Biochemicals; Indianapolis, IN).

Frozen brains from *gr/gr, mh/mh* and *gr/gr* mice were a generous gift of Dr. M. Burmeister (University of Michigan; Ann Arbor, MI). Brains were pulverized in liquid nitrogen. Extracts were thawed at 4°C in buffer A (150 mM NaCl, 20 mM HEPES, pH 7.4, 5 mM EGTA, 5 mM MgCl$_2$ 0.5) plus Complete antiproatease mixture and fractionated as described previously (van de Goor *et al.*, 1995). Synaptic vesicles were resolved in glycerol velocity gradients as mentioned above.

Immunomagnetic Isolations

PC12 SV isolated by glycerol velocity gradient (fractions 7–12) or rat brain SV were used in the assays. All the reactions and washes were done at 4°C in the presence of Complete antiprotease mixture. To detect differences in the distribution of SV antigens among vesicle subpopulations, reactions were designed so that the antibody-coated beads retained 20–40% of the vesicle input, except for those reactions performed with anti-HA antibodies where all ZnT3-HA was retrieved from the assay mixture. SV used as input pool controls were processed in identical conditions as the vesicles bound to beads except that beads and bovine serum albumin (BSA) were omitted. Dynabeads M-450 (Dynal, Oslo, Norway) were preincubated with antibodies either against LAMP II, synaptophysin, HA epitope, or VAMPII. Affinity-purified polyclonal antibody against ZnT3 1-78 was bound to Dynabeads M-280. Controls were performed in the presence of 50 μg of purified GST ZnT3 1-78 protein. All incubations and washes were done in PBS-BSA 5%. Vesicle binding to beads was made for 3 h at 4°C. Incubations were terminated by washing the beads four times for 10 min. Complexes were either processed for transmission electron microscopy or resolved by SDS-PAGE and analyzed by immunoblot. Immune complexes were detected by enhanced chemiluminescence. Multiple film exposures were obtained to determine ratios between VAMPII and synaptophysin. Band intensities were measured using the NIH Image 1.61 software (Grote *et al.*, 1995; Faundez *et al.*, 1997; Faundez and Kelly, 2000). To obtain a semiquantitative estimate of ratios in the blots, we included different amounts of the SLMV pool, so that the ratios between VAMP and synaptophysin were similar irrespective of the vesicle load. We determined the VAMP II/Synaptophysin ratios in the magnetically isolated membranes in the film where the VAMP II signals in the magnetically isolated vesicles were in the range of the VAMP II signal in SLMV ladder.

Cholesterol Depletion and Cell Surface Biotinylation

PC12 cells were washed in PBS and incubated in the absence or presence of 5 mg/ml (3.8 mM) or 10 mg/ml (7.6 mM) of MβCD during 45 min at 37°C in DMEM 0.3% fetal bovine serum (Thiele *et al.*, 2000). Cells were rinsed once with PBS and intracellular buffer at 4°C. SLMV protein contents were analyzed by immunoblot using equal amount of P1, P2 and P3 membrane pellets. Surface biotinylation with cleavable sulfo-NHS-SS-Biotin was made as described previously (Le Bivic *et al.*, 1989).

Other Procedures

Immunoprecipitations were performed as described previously (Grote *et al.*, 1995; Faundez *et al.*, 1997; Faundez and Kelly, 2000). Transferrin internalization assays were performed with Alexa 568-conjugated human transferrin (Molecular Probes) as described previously (Grote *et al.*, 1995; Faundez *et al.*,

1997; Faundez and Kelly, 2000). Brain cytosol was prepared from rat brain following established procedures (Clift-O'Grady *et al.*, 1998). Protein assays were performed using the Bio-Rad protein assay dye reagent (Bio-Rad, Hercules, CA) by using BSA as standard. All data are presented as average ± SE. Statistical analysis was performed using a two-tailed *t* test.

RESULTS

ZnT3 Interacts with the Adaptor Complex AP-3

Previous work by Kantheti *et al.* (1998) demonstrated that mossy fiber synaptic vesicles from AP-3–deficient mice lack both ionic vesicular zinc and its transporter, ZnT3. These observations suggest that ZnT3 is targeted to SV by an AP-3–dependent mechanism. To explore this hypothesis, we first analyzed whether AP-3 recognized cytosolic determinants of ZnT3. Purified GST-fusion proteins encoding both cytosolic domains of ZnT3, as well as the cytosolic synaptophysin carboxy-terminal domain, were used to perform affinity chromatography from brain cytosol. The synaptophysin carboxy-terminal tail fusion protein was used as a control because this domain is known to contain sorting information that targets synaptophysin to SLMV (Linstedt and Kelly, 1991a; Daly and Ziff, 2002). Binding of adaptor complexes to the fusion proteins was assessed by immunoblot by using adaptor-specific antibodies. Immunoblot analysis of protein complexes attached to beads revealed that AP-3 preferentially bound to the carboxy-terminal tail of ZnT3 (Figure 1A, lane 13). None of the GST fusion proteins bound detectable levels of AP-2 (our unpublished data).

Neuronal AP-3 is required for endosome-derived SLMV biogenesis in PC12 cells (Blumstein *et al.*, 2001). Therefore, we explored whether neuronal AP-3 could interact with the carboxy-terminal tail of ZnT3. Neuronal AP-3 complexes were assembled in HEK293 cells by transfection of the neuronal-specific isoforms β3b and μ3b, bearing myc and His6 tags at their COOH terminus. AP-3 complexes were immunoprecipitated using antibodies against the endogenous σ3 subunit. The presence of myc tagged β3b and μ3b subunits on the σ3 immunocomplexes was assessed by immunoblot by using myc antibodies. The tagged subunits were readily detectable in σ3 immunocomplexes (Figure 1B, lanes 5 and 6) but not in immunoprecipitates of a preimmune antibody (Figure 1C, lanes 2 and 3) indicating their incorporation into AP-3 complexes. Sucrose sedimentation analysis of detergent extracts from untransfected (Figure 1C, top) and transfected cells (Figure 1C, middle) showed that the hydrodynamic properties of endogenous AP-3 and complexes carrying the neuronal subunits were indistinguishable, thus suggesting that the free tagged subunits not incorporated into AP-3 tetramers were not recognized by myc antibodies. Neuronal AP-3 was immunoprecipitated from transfected HEK293 cells by using myc antibodies and the complexes were then tested for their ability to bind purified GST fusion proteins encompassing different domains of ZnT3 and synaptophysin (Figure 1D). Only beads containing neuronal AP-3 complex retained the COOH-terminal tail of ZnT3 (Figure 1D, compare lane 10 with 8 and 9). Neither the ZnT3 amino terminus nor the synaptophysin carboxy terminus bound to beads containing myc-tagged AP-3 complexes (Figure 1C, compare lane 10 with lanes 4 and 7). Thus, together, these results indicate that neuronal AP-3 directly interacts with the carboxy-terminal tail of ZnT3.

ZnT3 Targeting to PC12 SLMV

In PC12 cells, SLMV arise from the plasma membrane and from endosomes by AP-2– and AP-3–dependent pathways, respectively (Shi *et al.*, 1998; de Wit *et al.*, 1999). These mechanisms can be distinguished by treatment with BFA, a drug that
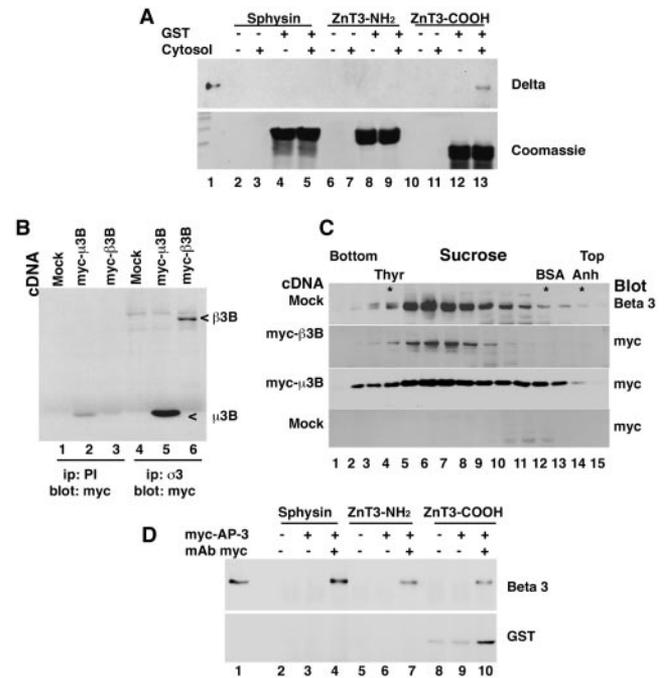

Figure 1. AP-3 interacts with the carboxy-terminal tail of ZnT3. (A) Glutathione beads were coated without (lanes 2, 3, 6, 7, 10, and 11) or with equal amounts of GST fusion proteins encompassing the carboxy-terminal cytosolic domain of synaptophysin (sphysin, lanes 4–5), the ZnT3 amino-terminal (lanes 8–9), and carboxy-terminal tails (lanes 12–13). Bead-bound fusion proteins were incubated in the absence (even lanes) or presence of rat brain cytosol (odd lanes). After washing, protein complexes bound to beads were analyzed by immunoblot with anti-delta antibodies (top) and the GST fusion proteins by Coomassie staining (bottom). Lane 1 represents 1/50 of the brain cytosol input. Only the carboxy-terminal tail of ZnT3 bound AP-3 from rat brain cytosol (n = 3). (B) Tagged neuronal AP-3 subunits are assembled in AP-3 complexes by HEK293 cells. HEK293 cells were transiently transfected with empty vector (lanes 1 and 4), myc-His6–tagged-μ3b (lanes 2 and 5), or myc-His6–tagged-β3b (lanes 3 and 6). Detergent cell extracts were immunoprecipitated using preimmune or σ3 antibodies, and the immunocomplexes were resolved in SDS-PAGE gels. Tagged subunits were detected in the immunoprecipitated material by using anti-myc 9E10 antibodies, indicating their incorporation into AP-3 complexes. (C) Tagged subunits incorporation into in AP-3 complexes was analyzed by sucrose gradient sedimentation (Dell'Angelica *et al.*, 1997) and compared with HEK293 endogenous AP-3 complexes. Immunoblots with β3 or myc epitope antibodies were used to identify the complexes. No differences in the sedimentation between endogenous AP-3 and AP-3 containing tagged subunits were detected. Thyroglobulin (Thyr, 669 kDa), albumin (BSA, 66 kDa), and carbonic anhydrase (Anh, 29 kDa) were used as molecular weight markers. (D) Neuronal AP-3 interacts with the carboxy-terminal tail of ZnT3. Myc-His6–tagged neuronal AP-3 reconstituted in HEK293 cells was bound to nonantibody-coated (lanes 2, 5, and 8) or 9E10 antibody-coated protein G beads (lanes 3, 4, 6, 7, 9, and 10). Lane 1 corresponds to input. Beads were incubated with equal amounts of the GST fusion proteins encoding the synaptophysin and ZnT3 cytosolic tails. After washing, complexes were resolved by SDS-PAGE and analyzed by immunoblot. Bound AP-3 and GST fusion proteins were detected with antibodies against the hinge domain of β3B and GST, respectively. Only the carboxy-terminal end of ZnT3 is retained by the neuronal AP-3 complex (n = 3).

halts AP-3–dependent, but not AP-2–dependent, SLMV biogenesis (Faundez *et al.*, 1997; Shi *et al.*, 1998). To test whether ZnT3 is trafficked by the AP-3 pathway, we examined the

effects of BFA on the subcellular distribution of both endogenous and transfected ZnT3 protein in PC12 cells.

We first determined whether ZnT3 was present in PC12 early endosomes by labeling them by a short pulse of Alexa-conjugated transferrin. Due to the low endogenous levels of ZnT3, we used PC12 cells expressing ZnT3-GFP. This construct was properly targeted to endosomes and SLMV compared with the endogenous ZnT3 or a ZnT3 carrying a smaller HA tag (our unpublished data). ZnT3-GFP expression was prominent in the perinuclear area where it strongly colocalized with internalized transferrin (Figure 2A), thus indicating that the perinuclear pool of ZnT3 is present in early endosomes.

Newly formed vesicles derived from endosomes disappear with a half-life of 36 min after BFA block (Faundez *et al.*, 1997). Thus, we predicted that after 2 h in the presence of the drug, proteins trafficked by this pathway should decrease markedly in SLMV. PC12 cells expressing HA-ZnT3 were incubated in the absence or presence of BFA. Control and BFA-treated cell postnuclear supernatants (S1) were sedimented in velocity sucrose gradients to resolve SLMV (fractions 12–15) (Lichtenstein *et al.*, 1998) (Figure 2, B–G). In untreated cells, ZnT3-HA (Figure 2B) or endogenous ZnT3 (Figure 2F) were readily detectable in SLMV (fractions 12–15), yet BFA treatment substantially decreased the ZnT3 content in these fractions (Figure 2, C and G, n = 3). In contrast, as described previously, the synaptophysin content was only minimally perturbed by BFA (Blagoveshchenskaya *et al.*, 1999) (Figure 2, D and E), suggesting that different SLMV sorting mechanisms control synaptophysin and ZnT3. ZnT3 was redistributed from the membranes present in S1 to the P1 pellet. After drug treatment, ZnT3 but not synaptophysin content per microgram of P1 membranes increased moderately (Figure 2H) because reallocated ZnT3 was diluted into a P1 pellet that contains 75% of membrane proteins present in the cell. The BFA-induced change in ZnT3 subcellular distribution was also observed by time-lapse confocal microscopy. Consistent with the redistribution of ZnT3 to the P1 pellet, ZnT3-GFP progressively accumulated around the perinuclear area after BFA treatment (Figure 2I).

Thus, together, our data are consistent with the hypothesis that ZnT3 is trafficked from endosomes by the AP-3 pathway.

Differential Effects of Methyl-β-Cyclodextrin upon Synaptic Vesicle Protein Targeting

Cholesterol depletion by methyl-β-cyclodextrin (MBCD) arrests clathrin-AP-2–dependent vesicle formation (Rodal *et al.*, 1999; Subtil *et al.*, 1999; Wu *et al.*, 2001) and, in PC12 cells, halts the biogenesis of synaptophysin-containing SLMV from plasma membrane (Thiele *et al.*, 2000). Because endosomes are not perturbed by cholesterol depletion (Rodal *et al.*, 1999; Subtil *et al.*, 1999; Wu *et al.*, 2001), we hypothesized that plasma membrane and endosome-derived SLMV biogenesis mechanisms could be differentially modulated by cholesterol depletion. To test this, membrane fractions were isolated from MBCD-treated or control PC12 cells and assayed for the presence of marker proteins. In untreated controls, synaptophysin was concentrated in an SLMV-enriched membrane fraction (P3) as expected. In contrast, cells incubated in the presence of MBCD showed decreased targeting of synaptophysin to SLMV (Figure 3A, P3) as described previously (Thiele *et al.*, 2000). This effect on synaptophysin was not due to a generalized inhibition of all endocytic events because neither the distribution of the transferrin receptor (Thiele *et al.*, 2000), which undergoes receptor-mediated endocytosis from the plasma membrane, nor the SLMV levels of ZnT3 were substantially affected by
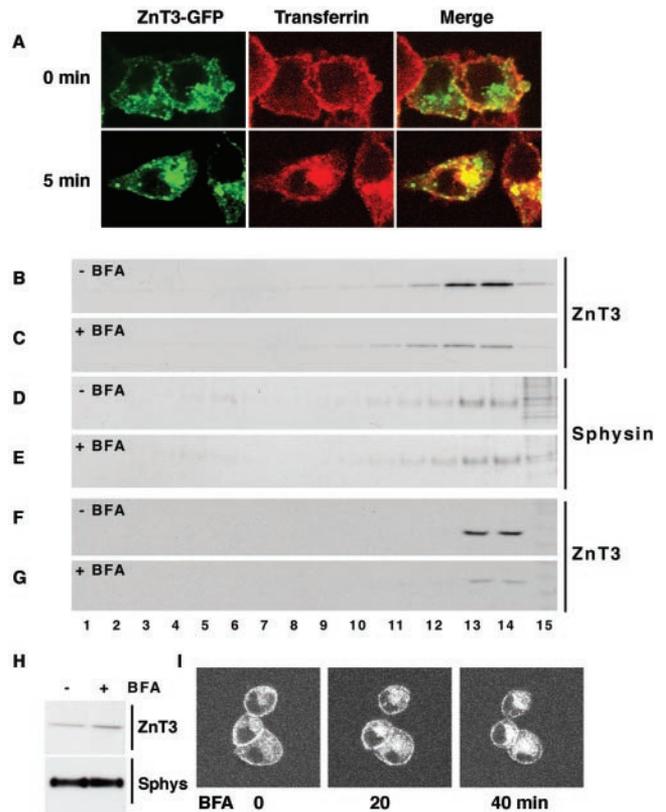

Figure 2. ZnT3 targeting from endosomes is perturbed by brefeldin A. (A) ZnT3 is localized in early endosomes. To label cell surface, PC12 cells carrying ZnT3-GFP were incubated at 4°C with Alexa568-transferrin (50 μg/ml) and washed to remove unbound ligand. Cell were kept either at 4°C or transferred to 37°C to resume internalization. Assays were stopped at 0°C. Perinuclear ZnT3 is extensively decorated by internalized transferrin, indicating its early endosome nature. (B–G) Brefeldin A preferentially hinders ZnT3-HA targeting to SLMV. ZnT3 clone 4 PC12 cells (B–E) or untransfected PC12 cells (F and G) were incubated in the absence (B, D, and F) or presence of brefeldin A (10 μg/ml; C, E, and G) for 2 h. Cells were homogenized and equal protein amounts of SLMV-enriched S1 supernatants were resolved in 10–45% sucrose velocity gradients (Lichtenstein *et al.*, 1998). Fractions were analyzed by immunoblot with antibodies against synaptophysin (sphysin) and ZnT3. Although SLMV synaptophysin content was minimally affected by brefeldin A, ZnT3 was robustly reduced. Brefeldin A reduces the targeting of endogenous ZnT3 to SLMV (compare F and G). (H) ZnT3 present in SLMV is redistributed to P1 membranes were ZnT3 content increases after drug treatment. (I) Endosomal ZnT3-GFP perinuclear distribution is modified by brefeldin A. PC12 cells transfected with ZnT3-GFP were incubated at 37°C in the presence of brefeldin A (10 μg/ml) and imaged by time-lapse confocal microscopy. Time 0 represents a frame taken before the addition of the drug. Brefeldin A induced a redistribution of ZnT3-GFP. Shown a representative section from a Z-time series (n = 3).

cholesterol depletion (Figure 3, B and D). To confirm that the effects of MBCD upon the synaptophysin-content on P3 membranes were indeed in SLMV, we resolved P3 membranes by glycerol velocity sedimentation (Figure 3C). After MBCD treatment, the synaptophysin content in SLMV was dramatically reduced, whereas BFA treatment did not decrease its content (Figure 3C). In contrast, under identical conditions, SLMV ZnT3 was pronouncedly decreased by BFA treatment, yet the transporter targeting to SLMV was not impaired by cholesterol depletion (Figure 3C). Identical

Figure 3. Differential effects of plasma membrane cholesterol depletion upon synaptic vesicle protein targeting to SLMV. (A) PC12 cells were incubated in the absence or presence of MBCD (10 mg/ml) for 45 min at 37°C to deplete plasma membrane cholesterol. Incubations were stopped at 4°C and cell homogenates fractionated as described in MATERIALS AND METHODS. Equal protein amounts from pellets P1–P3 were resolved on SDS-PAGE gels and the distribution of TfR and synaptophysin (sphysin) was determined by immunoblot. P3 pellets were substantially enriched in SV markers, yet devoid of detectable transferrin receptor. Synaptophysin content on SLMV (P3) was substantially reduced after MBCD. (B) Cholesterol depletion does not modify the intracellular pool of transferrin receptor. PC12 cells were biotinylated at 4°C with the disulfide cleavable biotinylation agent NHS-Biotin. Cells were warmed to 37°C, in either the absence or presence of MBCD for 45 min. Reactions were stopped and the cell surface biotin was removed with glutathione at 4°C. Cell extracts were precipitated with streptavidin-agarose beads and the presence of transferrin receptor was assessed by immunoblot. No differences in the intracellular pool of transferrin receptor were detected, therefore excluding a generalized endocytic trafficking defect induced by cholesterol depletion. (C) Cholesterol depletion selectively reduces synaptophysin targeting to SLMV. PC12 cells transfected with ZnT3-HA were treated in the absence or presence

MBCD (10 mg/ml) or BFA (10 μg/ml). Reactions were stopped in ice and equal protein amounts of cell homogenate were resolved by differential and glycerol gradient centrifugation. SLMV content of synaptophysin and ZnT3 were determined by immunoblot. In contrast to ZnT3, synaptophysin targeting is affected by cholesterol depletion but not by BFA (n = 3). (D) ZnT3 targeting to SLMV is not affected by cholesterol depletion in P3 membranes. Untransfected PC12 or cells transfected with ZnT3-HA were treated or not with MBCD. Equal amounts of P3 protein were analyzed by immunoblot. Although the synaptophysin content on P3 vesicles was substantially reduced after MBCD treatment, both endogenous (ZnT3) and HA-tagged ZnT3 (ZnT3-HA) did not exhibit decreased content on SLMV after cholesterol depletion. (E) Results expressed as percentages of the control value obtained in the D). (F) Cholesterol depletion affects the SLMV targeting of different SV proteins. PC12 cells or a clone bearing Vglut1 were treated with increasing concentrations MBCD. P3 SLMV were isolated and their content of synaptophysin (sphysin), VAMP II, ClC3, and Vglut1 was determined by immunoblot on equal amounts of P3 protein. Results are expressed as percentages of the control value. SLMV protein contents in the absence of drug were arbitrarily set to 100%. PC12Vglut1 (n = 2), PC12 (n = 7), and PC12 ZnT3-HA (n = 3). Absent error bars correspond to errors below the graphing threshold.
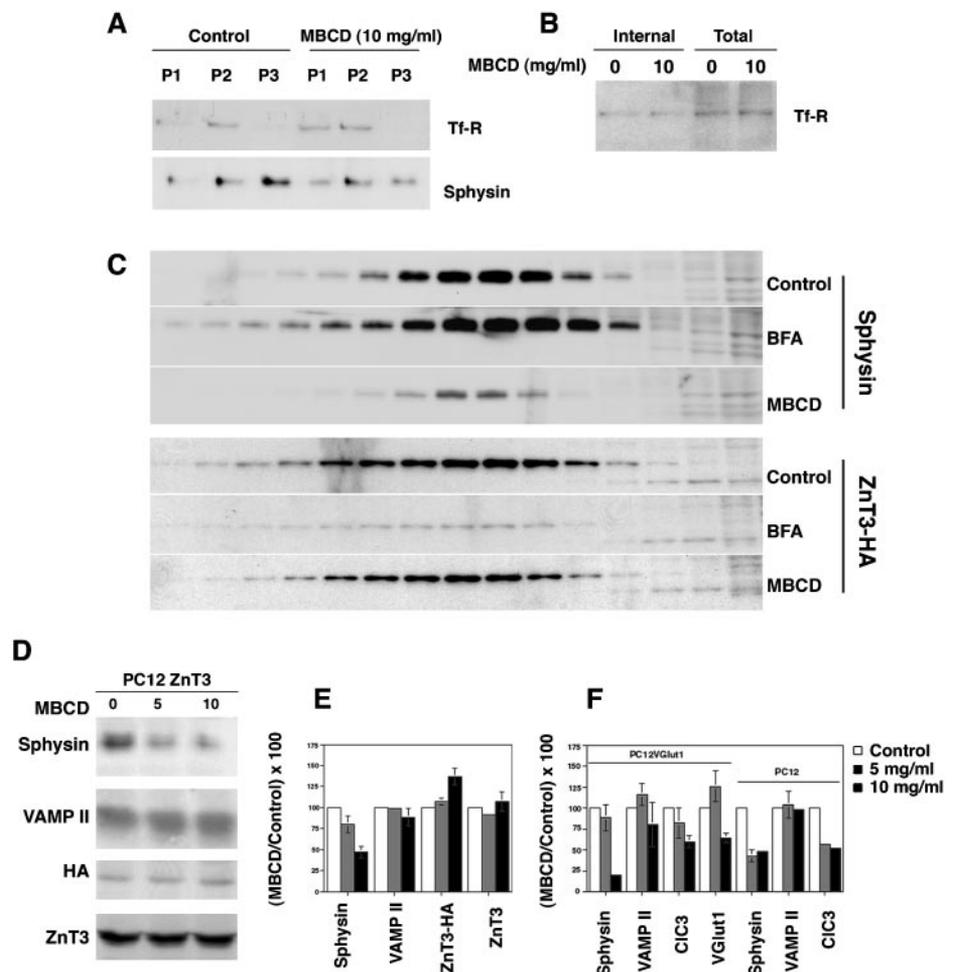
results were obtained whether P3 or glycerol gradient resolved membranes were analyzed (Figure 3, C and D).

In all the PC12 cell lines tested, synaptophysin targeting to SLMV assessed in P3 membranes was dramatically reduced after MBCD treatment to a 35.9 ± 7% of control values (Figure 3, E and F). In contrast to synaptophysin, the level of endogenous ZnT3 in SLMV was not altered under identical conditions of MBCD treatment (107 ± 11.5%, n = 3). In fact, transfected ZnT3-HA increased 37% in MBCD-treated SLMV (137 ± 9.7%, n = 3 p < 0.02) relative to untreated controls (Figure 3D–F). Plasma membrane cholesterol depletion effects were also seen with other SLMV proteins. VAMP II was reduced to 89 ± 5.1% (p < 0.02) (Figure 3, E and F), whereas the targeting of the chloride channel 3 (ClC3) (Stobrawa *et al.*, 2001) and the synaptic vesicle glutamate transporter (Vglut1) (Bellocchio *et al.*, 2000; Takamori *et al.*, 2000) to SLMV was decreased to 60 ± 6.9% (n = 4) and 64 ± 5.4%

(n = 2) of control values, respectively (Figure 3F). This intermediate effect was striking and could be explained if ClC3 and Vglut1 are found both in SLMV derived from plasma membrane and endosomes. Thus, the pronounced MBCD effect upon synaptophysin is likely due to a block in plasma membrane-derived SLMV biogenesis rather than to a synaptophysin-specific sorting defect. These results suggest that MBCD treatment modifies the biogenesis of vesicles from the plasma membrane. Furthermore, they are consistent with a model of two SLMV biogenesis pathways that assemble vesicles of different composition.

ZnT3 and Synaptophysin Are Enriched in Different SLMV Subpopulations

If all vesicles in a SLMV pool possess identical composition, then regardless of the antibody used to isolate the vesicles, the ratio of different SV markers should remain the same.
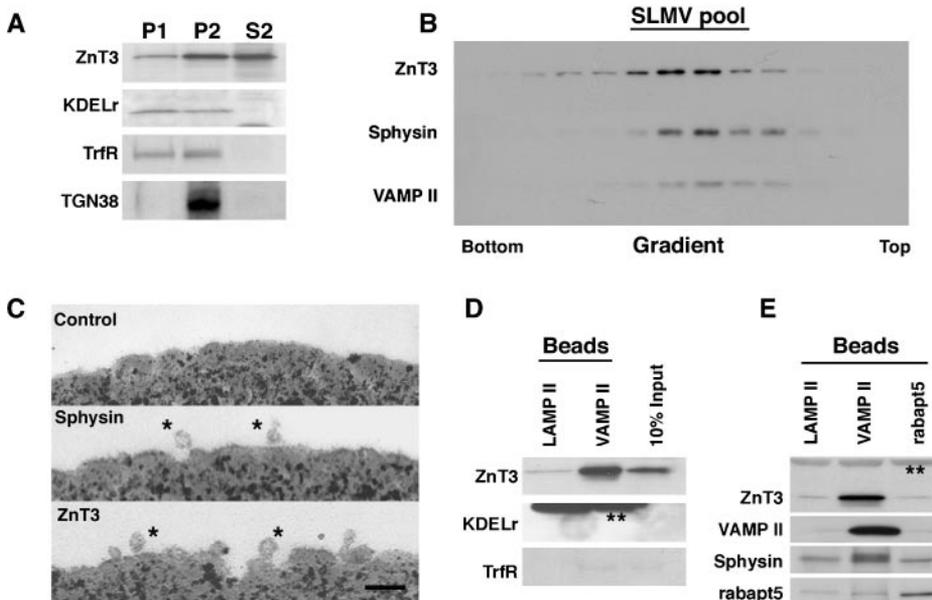
Figure 4. Biochemical and ultra-structural characterization of the ZnT3 and synaptophysin-containing SLMV. (A) PC12 clone 4 cell expressing ZnT3-HA were differentially fractionated to generate P1, P2, and SLMV-enriched S2 fractions. Equal protein amounts of these fractions were resolved in SDS-PAGE and tested by immunoblot with antibodies against ZnT3, KDELr, TrfR, and TGN38. S2 fraction does not contain appreciable contamination with exocytic or endocytic membranes. (B) SLMV-enriched S2 fractions from PC12 clone 4 cells were size fractionated in 5–25% glycerol gradients and probed with antibodies against synaptophysin, VAMP II, and ZnT3. All SV proteins comigrated on the same region of the gradient. (C) Magnetic beads coated with anti-LAMP II antibodies (control), anti-synaptophysin, and anti-HA tag (ZnT3) were incubated with glycerol gradient-purified vesicles (SMLV pool, B). Beads were extensively washed and processed for transmission electron microscopy. Asterisks mark isolated vesicles bound over the horizon of the magnetic bead. Size distribution analysis of these vesicles was identical for ZnT3 and synaptophysin isolated SLMV. (D) and E) SLMV were isolated with control beads coated with an antibody against LAMP II or with antibodies against VAMP II or rabaptin 5 (rabapt5). Beads bound membranes were resolved by SDS-PAGE and analyzed by immunoblot against the antigens described in the figure. VAMP II concentrated SLMV as assessed by ZnT3, VAMP II, and synaptophysin immunoreactivity but not other membranes. Rabaptin 5-coated beads did not enriched SLMV markers. Double asterisks denote IgG chains.

Conversely, if SLMV of different composition are present in the SLMV pool, antibodies specific for markers of different types of SLMV could bring down vesicles that differ in the ratios of SV protein markers. However, vesicles that differ in the ratios of their SV protein components could be also explained by the presence of contaminant, non-SLMV membranes. Consequently, we first asked whether markers of exocytic or endocytic membranes could be found in our purified SLMV (Figure 4). PC12 homogenates were differentially fractionated to obtain SLMV-rich S2 supernatants (Figure 4A). Although S2 membranes contained significant levels of the SV protein ZnT3 (Figure 4A), we did not detect endoplasmic reticulum, early endosomes, and *trans*-Golgi network-derived membranes as determined with antibodies against the KDEL receptor (KDELr), transferrin receptor (TfrR), and TGN38, respectively. The SLMV-enriched S2 membranes were further resolved in glycerol gradients to isolate SLMV (Figure 4B). Vesicles were identified by the migration of the synaptic vesicle markers ZnT3, VAMP II, and synaptophysin. All of these markers comigrated in the center of glycerol gradients (Figure 4A), indicating that synaptic vesicle antigens are targeted to homogeneously sized vesicles whose physical properties were similar to brain SV (Figure 4A) (Clift-O'Grady *et al.*, 1990; Schmidt *et al.*, 1997). We characterized the SLMV isolated from glycerol gradients by electron microscopy (Figure 4C). SLMV were pooled from glycerol gradients (Figure 4B), and membranes were incubated with magnetic beads carrying antibodies to the cytosolic tails of synaptophysin, ZnT3, or a luminal LAMPII epitope as a control. Bead-bound vesicles were then examined by transmission electron microscopy, and vesicle diameters were determined. Consistent with the glycerol gradient results, no differences in the size of synaptophysin-isolated (30.1 ± 7 nm; n = 43) and ZnT3-isolated SLMV (29.7 ± 6 nm; n = 187) were detected. SLMV isolated with magnetic beads coated with antibodies against VAMP II retrieved vesicles

containing ZnT3 yet devoid of detectable KDEL receptor (Figure 4D), rabaptin 5, EEA1, and rab5 (our unpublished data). We estimated that bead bound vesicles contained <10% of transferrin positive membranes (Figure 4D). Conversely, anti rabaptin 5-coated and control LAMP II-coated beads retrieved SLMV antigens to a similar extent (Figure 5E). These findings are consistent with previous reports (Clift-O'Grady *et al.*, 1990; Linstedt and Kelly, 1991b; Bonzelius *et al.*, 1994; Herman *et al.*, 1994; Lichtenstein *et al.*, 1998; de Wit *et al.*, 1999, 2001) and demonstrate that our isolated PC12 SLMV are reasonably devoid of other contaminant vesicles.

To determine whether different populations of vesicles existed within the SLMV pool, we used magnetic beads coated with antibodies against the tails of either ZnT3, synaptophysin, or VAMP II to isolate vesicles from our PC12 SLMV (see SLVM pool in Figure 4B). The protein composition of the isolated vesicles was assessed by immunoblot and compared with the contents of the pooled purified SLMV. To detect differences in the distribution of SV antigens among vesicle subpopulations, reactions were designed so that the beads contained sufficient antibody to bind 20–40% of the vesicle input (Figure 5, A and B).

VAMP II bearing the mutation N49A exhibits an enhanced AP-3–dependent sorting to SLMV compared with wild type, and thus should be enriched in vesicles derived from the AP-3 pathway (Grote *et al.*, 1995; Salem *et al.*, 1998). We magnetically isolated SLMV purified from PC12 VAMP II N49A cells by using well-characterized monoclonal antibodies against the cytosolic tails of synaptophysin (Wiedenmann and Franke, 1985) and VAMP II (Baumert *et al.*, 1989). Control beads coated with human-specific antibodies against the luminal domain of LAMP II, a lysosomal antigen, did not retrieve SLMV antigens. In contrast, beads coated with synaptophysin and beads carrying VAMP II antibodies both recovered SV antigens, although in different ratios (Fig-
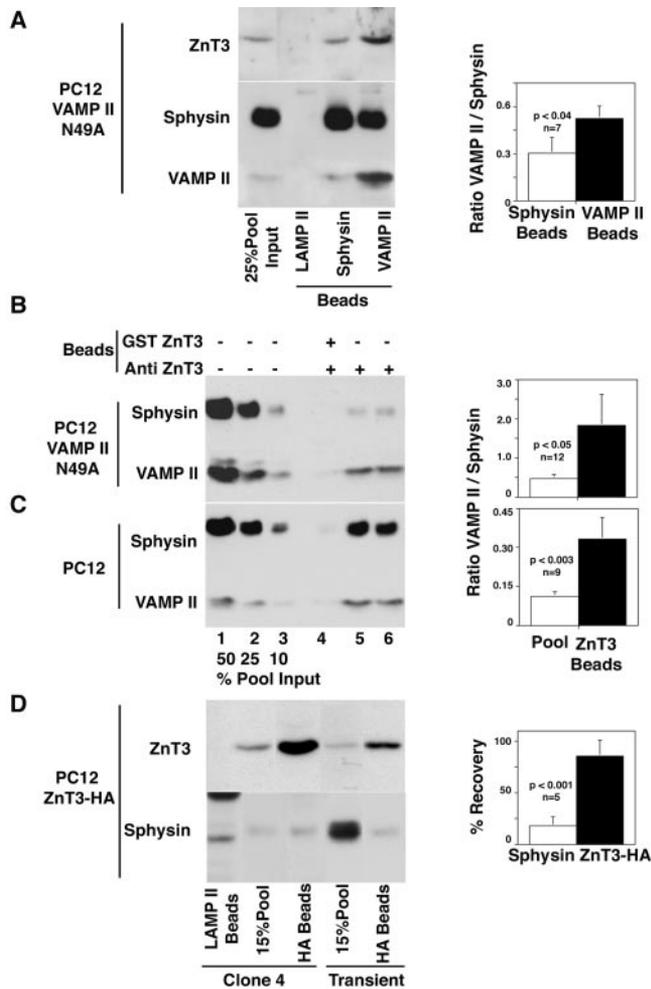
A

PC12
VAMP II
N49A

ZnT3

Sphysin

VAMP II

25%Pool Input | LAMP II | Sphysin | VAMP II

Beads

Ratio VAMP II / Sphysin

p < 0.04
n=7

Sphysin Beads | VAMP II Beads

B

Beads | GST ZnT3 | - - - + - -
Anti ZnT3 | - - - + + +

PC12
VAMP II
N49A

Sphysin

VAMP II

C

PC12

Sphysin

VAMP II

1 2 3 4 5 6
50 25 10
% Pool Input

Ratio VAMP II / Sphysin

p < 0.05
n=12

Pool | ZnT3 Beads

p < 0.003
n=9

D

PC12
ZnT3-HA

ZnT3

Sphysin

LAMP II Beads | 15%Pool | HA Beads | 15%Pool | HA Beads

Clone 4 | Transient

% Recovery

p < 0.001
n=5

Sphysin | ZnT3-HA

Figure 5. ZnT3 and synaptophysin are enriched in different SLMV populations. (A) Glycerol gradient isolated SLMV derived from PC12 VAMP II N49A cells were immuno-magnetically isolated with beads coated with control (LAMP II), synaptophysin, or VAMP II antibodies. After washing, bead-bound immuno-complexes were resolved in SDS-PAGE gels and analyzed by immunoblot with antibodies against VAMP II and synaptophysin. Isolations performed with VAMP II antibodies consistently brought down vesicles enriched in VAMP II over synaptophysin compared with vesicles isolated with synaptophysin antibodies. Control beads did not bind SLMV. First lane from the left represents 25% of the vesicle input. Quantifications of seven assays performed in three independent experiments are shown to the right. Glycerol gradient-isolated SLMV derived from PC12 VAMP II N49A cells (B) or untransfected PC12 cells (C) were immuno-magnetically isolated with beads coated with affinity-purified anti-ZnT3 amino-terminal antibodies. Controls were performed by competing vesicle binding with an excess of the ZnT3 amino-terminal GST fusion protein. Immuno-complexes were resolved by SDS-PAGE and analyzed by immunoblot. Depicted from left to right are decreasing concentrations of the SLMV input (percentage of the total), control reaction competed with the amino-terminal tail of ZnT3, and two immuno-magnetic anti-ZnT3 isolations. ZnT3 isolated vesicles are enriched in VAMP II over synaptophysin at least threefold compared with the SLMV pool. Right, quantifications of 12 and 9 assays performed in four and three independent experiments, respectively. (D) Glycerol gradient isolated SLMV derived from PC12 ZnT3-HA clone 4 cells or transiently transfected cells were immuno-magnetically isolated with beads coated with control (LAMP II, first lane from the left) or anti-HA antibodies. Although nearly all ZnT3-HA-containing vesicles were isolated with anti-HA antibodies, the immuno-magnetic beads only retrieved a 17% of all the vesicle-bound synaptophysin

ure 5A). On average, the ratio of VAMPII/synaptophysin was 1.7 times higher in vesicles isolated with VAMP II antibodies than those isolated with anti-synaptophysin. Concomitantly, ZnT3 content was increased in the N49A vesicles isolated with VAMP II antibodies compared with those isolated with synaptophysin antibodies (Figure 5A). This suggests that some VAMPII is present in vesicles that are relatively poor in synaptophysin and enriched in ZnT3 content. PC12 N49A SLMV were also isolated using beads coated with affinity-purified antibodies against the ZnT3 NH-terminal tail (Figure 5B). Vesicles isolated using these ZnT3 antibodies exhibited a fourfold increased content of VAMP II per unit of synaptophysin with respect to the starting SLMV pool (Figure 5B, compare the amount of VAMP II in lanes 5 and 6 with lane 3, all of which possess similar synaptophysin content), supporting the hypothesis that ZnT3 is enriched in a distinct subpopulation of vesicles. Synaptophysin and VAMP II signals were not detected in isolations performed in the presence of competing ZnT3 fusion protein, demonstrating the specificity of the ZnT3 antibody. This enrichment of VAMP II over synaptophysin was not restricted to the PC12 N49A cell line. ZnT3 antibodies were used to isolate vesicles from an SLMV pool prepared from normal PC12 cells (Figure 5C). In this case, the total VAMPII signal is lower relative to total synaptophysin because of the lower expression levels of the endogenous VAMPII protein compared with the transfected VAMPII N49A (Figure 5B). Nonetheless, the ZnT3-isolated vesicles were enriched in their endogenous VAMP II content threefold relative to the starting pool (Figure 5C, compare the amount of VAMP II in lanes 5 and 6 with lane 2, all of which possess similar synaptophysin content).

We further tested the hypothesis that ZnT3 and synaptophysin were segregated to different SLMV populations by using PC12 cell lines expressing an HA-tagged derivative of ZnT3 (Figure 5C). SLMV prepared from these clones contained 10-fold more ZnT3 than the starting cell line. Vesicles isolated from this SLMV pool by using anti-HA antibodies contained the majority of the ZnT3 present in the original SLMV population (85.8 ± 14.9%; n = 5). However, only one-sixth of the total synaptophysin input was recovered (17.6 ± 9%; n = 5). Similar results were obtained in two different clonal HA-ZnT3 cell lines as well as in the PC12 cells transiently transfected with HA-ZnT3. Thus, even under conditions of overexpression, ZnT3 and synaptophysin are enriched in different vesicular compartments that bear the properties of SLMV.

ZnT3 and Synaptophysin Are Enriched in Different Populations of Brain SV

To assess heterogeneities in synaptic vesicle antigen distribution, we analyzed by confocal immunomicroscopy the distribution of ZnT3, VAMP II, and synaptophysin in neuronal processes of cultured hippocampal neurons (Figure 6). Affinity-purified anti-ZnT3 antibodies recognized a single band in ZnT3-transfected but not ZnT4-transfected cells (our unpublished data). Moreover, although these antibodies strongly stained hippocampal mossy fiber terminals, they

---

protein present in the assay. Low levels of synaptophysin were also detected in SLMV isolated with anti-HA antibodies, by using vesicles purified from transiently transfected cells. Quantifications of five assays performed in three independent experiments with SLMV derived from clone 4 are shown at the right. Values represent the percentage of recovery of the total amount of vesicle-bound ZnT3 and synaptophysin added to the assay.
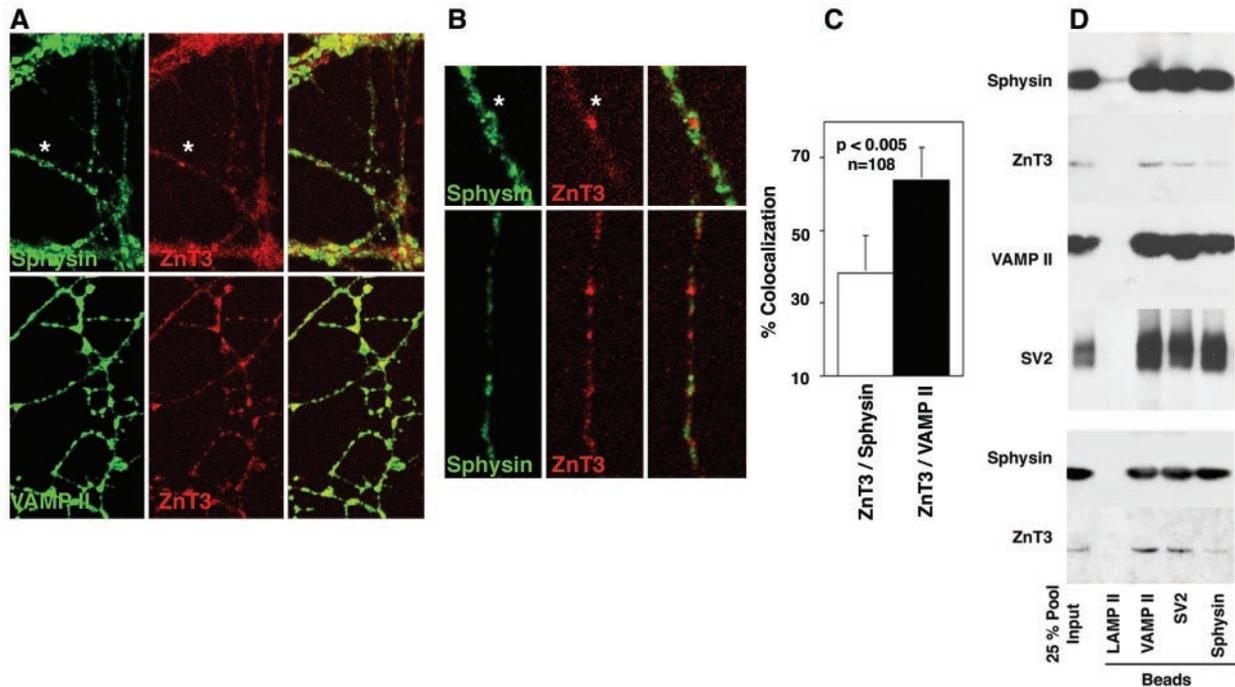
Figure 6. Localization of ZnT3 and SV antigens in primary cultures of hippocampal neurons. Primary cultures of hippocampal neurons (14 DIV) were double stained with antibodies against ZnT3, synaptophysin, or VAMP II antibodies. Images of the processes were acquired by confocal microscopy. (B) Magnification of the area marked by an asterisk in A, and a process from a field obtained in an independent experiment. Asterisk show regions positive for ZnT3, but with reduced levels of synaptophysin immunoreactivity. The extent of colocalization was determined in single optical sections of isolated processes (14 DIV). (C) Quantification of the extent of colocalization between ZnT3 and the other SV antigens by using MetaMorph. (D) Purified brain SV were immuno-magnetically isolated with beads coated with control (LAMP II), synaptophysin, SV2, or VAMP II antibodies. Beads were washed and immuno-complexes were resolved in SDS-PAGE gels and analyzed by immunoblot with antibodies against ZnT3, VAMP II, SV2, and synaptophysin. Isolations performed with VAMP II and SV2 antibodies consistently brought down vesicles containing ZnT3. In contrast, isolations performed with synaptophysin antibodies retrieved low levels of vesicle-associated ZnT3. Control beads did not bind SV. First lane from the left represents 25% of the vesicle input. Depicted are two representative experiments of four performed at least in duplicate. Two independent SV preparations were used (top and bottom).

did not recognize cell bodies or the surrounding neuropil of rat hippocampal sections (our unpublished data).

Anti-synaptophysin and VAMP II antibodies robustly decorated the neuropil of 14-d cultured hippocampal neurons. ZnT3 antibodies also stained these processes, although to a lesser extent compared with VAMP II or synaptophysin (Figure 6A). This was entirely consistent with the relative signal levels observed on immunoblots (Figure 6D). ZnT3 immunoreactivity evidenced extensive colocalization with VAMP II. In contrast, we observed neurites where ZnT3-positive domains were poorly decorated with synaptophysin immuno-reactive material (Figure 6, A and B, asterisks). Using MetaMorph software, we quantitated the percentage of colocalization between the different SV markers (Figure 6C). About two-fifths of the synaptophysin-positive regions (38 $\pm$ 10.5%) were also positive for ZnT3, whereas 64 $\pm$ 9% of those positive for VAMP II colocalized with ZnT3 (n = 108 fields acquired in four independent experiments).

Synaptic vesicle proteins travel along the axon in distinct precursor membranes; thus, differences in antigen colocalization along processes could in addition reflect differences in their distribution among membranes upstream of synaptic vesicle biogenesis. We therefore determined whether differential SV antigen partitioning was evident in purified rat brain SV (Figure 6D). ZnT3 protein was detected in vesicles isolated using antibodies to either VAMP II or SV2. However, SV isolated with anti-synaptophysin-coated beads contained low

amounts of ZnT3. These low ZnT3 levels were not due to a disruption of the vesicles isolated with synaptophysin antibodies because similar levels of synaptophysin, VAMP II, and SV2 were obtained irrespective of the antibody used to isolate the vesicles. These results indicate that ZnT3 and synaptophysin are preferentially targeted to distinct brains SV populations. If ZnT3 and synaptophysin are targeted to different synaptic vesicles due to their differential interaction with AP-3 (Figure 1), then AP-3 adaptor deficiencies should ablate ZnT3 from vesicles without affecting the carrier population containing synaptophysin. We tested this hypothesis by analyzing ZnT3 and synaptophysin content in SV derived from wild-type and AP-3–deficient mouse brains. SV content of ZnT3 and synaptophysin were assessed by immunoblot of membrane fractions resolved in glycerol gradients. In these gradients, synaptophysin levels in synaptic vesicles remained constant irrespective whether the vesicles were isolated from wild-type or *mocha* brains (Figure 7A). In contrast, ZnT3 content was reduced in vesicles isolated from AP-3–deficient brains (Figure 7A). Surprisingly, we observed a generalized, yet selective, reduction in the ZnT3 content in larger brain membranes (Figure 7B, P1 and P2). Irrespective whether we analyzed the ZnT3 content in SV or larger membranes we observed a reduction of ~80% (Figure 7C). Impairing the formation of PC12 AP-3–derived SLMV by BFA did not modify the total cellular levels of ZnT3 (Figure 7D). These results show that a normal ZnT3 SV content, but not synaptophysin, relies in an AP-3–dependent mechanism.
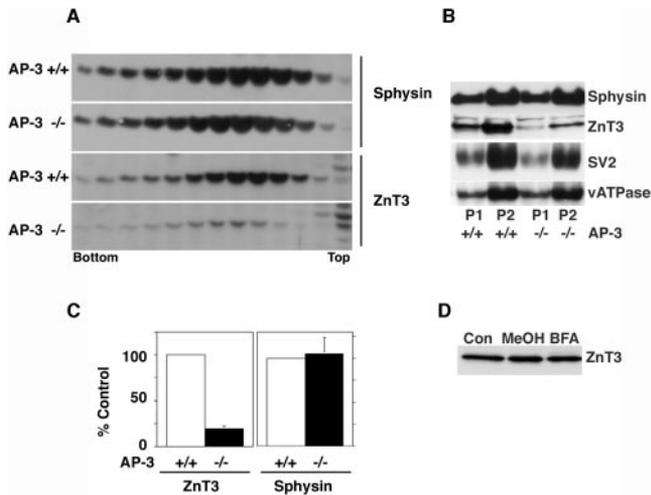
Figure 7. ZnT3 and synaptophysin targeting to synaptic vesicles from AP-3–deficient mouse. High-speed supernatants obtained from wild-type and *mocha* brains were sedimented in 5–25% glycerol velocity gradients to resolve SV. SV were identified by immunoblot with antibodies against synaptophysin (sphysin) and ZnT3. (A) In contrast to synaptophysin SV, ZnT3 content is decreased in AP-3 deficiencies. (B) Immunoblot analysis of synaptophysin, ZnT3, SV2, and the p116 subunit of the vacuolar ATPase in P1 and P2 membranes of wild-type and *mocha* brain membranes. ZnT3 is the only SV antigen whose levels are affected by the *mocha* allele. (C) Quantitation of ZnT3 and synaptophysin content in the synaptic vesicle peak (fractions 7–9) in four independent experiments. A similar decrease in ZnT3 content was observed by quantifying the transporter in P1 or P2 membranes (n = 5). (D) Brefeldin A-induced block in ZnT3 targeting to SLMV does not decrease the total cellular levels of ZnT3. PC12 ZnT3-HA clone 4 cells were incubated with BFA as described in Figures 1 and 2. The total cellular levels of ZnT3 were determined by immunoblot. ZnT3 cell content remained constant in the presence of BFA (n = 2).

Zinquin, a Zinc-sensitive Probe, Reveals Heterogeneity in Neuronal Vesicular Stores

To monitor in vivo the function of ZnT3 in hippocampal neurons, we used as an indicator the vesicular ionic zinc stores. The rationale for selecting ionic zinc as a tool was based in the following observations: 1) disruption of the ZnT3 gene in mouse leads to a disappearance of all detectable ionic zinc in neurons (Cole *et al.*, 1999), indicating that ZnT3 is the main vesicular ionic zinc transport mechanism in brain; and 2) AP-3–deficient neurons do not store vesicular ionic zinc (Kantheti *et al.*, 1998) because of a lack of ZnT3 in their SV (Kantheti *et al.*, 1998) (Figure 7). Because SV uptake of ionic zinc increases intravesicular pH (Goncalves *et al.*, 1999), we hypothesized that if vesicles differ in their ZnT3 content or function, then differences in the vesicular pH should be detectable on single terminals. To explore this hypothesis, we determined, in cultured hippocampal neurons, both the vesicular ionic zinc content, by using the zinc-specific, fluoroprobe zinquin (Zalewski *et al.*, 1993, 1994; Snitsarev *et al.*, 2001) and the vesicular pH with Lyso-Sensor Green DND-189. This dye stains plasma membrane and acidic compartments and possesses a pK_a identical to the SV intravesicular pH (pH 5.2) (Lin *et al.*, 2001).

Both zinquin and LysoSensor Green stained processes and boutons of isolated hippocampal neurons (Figure 8, A and B). Zinquin- and Lysosensor-positive compartments correspond to vesicles that undergo regulated secretion, as revealed by their redistribution from hippocampal neuronal

processes after α-latrotoxin treatment (Figure 8A). α-Latrotoxin induced a rapid redistribution of LysoSensor signal from intracellular compartments to the plasma membrane, whereas the zinquin fluorescence decayed to 67 ± 9.6% after 2 min of treatment (32 boutons, three independent experiments). In contrast, zinquin fluorescence loss in the absence of α-latrotoxin was 16 ± 7% (n = 15 boutons, two independent experiments). Incubating the neurons with bafilomycin A1, a vacuolar ATPase blocker known to deplete SV of their contents (Zhou *et al.*, 2000), abrogated zinquin and LysoSensor signals (our unpublished data). Rather than a homogeneous costaining with both dyes, neuronal processes and boutons were interspersed with either zinquin (Figure 8B, arrowheads), LysoSensor (Figure 8B, arrows), or double-labeled segments. Frequently, we observed boutons labeled only with zinquin (Figure 8B, arrowheads, bottom). These results suggest that zinc transport defines vesicle pools that differ in their intravesicular pH and support the notion of heterogeneity in secretory vesicle compartments.

DISCUSSION

The analysis of synaptophysin and ZnT3 targeting to PC12 cell SLMV or SV derived from wild-type or AP-3–deficient brain supports the hypothesis that different adaptor-dependent mechanisms generate distinct, but overlapping, populations of vesicles.

We have used variants of the PC12 cell line as homogeneous, single cell-type model systems to biochemically characterize the routes that ZnT3 and synaptophysin take to reach SV. This cell line possesses both AP-2 and AP-3 SV biogenesis pathways (Faundez *et al.*, 1997, 1998; Shi *et al.*, 1998; de Wit *et al.*, 1999). AP-3–dependent SV biogenesis generates new SV from endosomes by an ARF1-dependent mechanism (Faundez *et al.*, 1997, 1998). This pathway is potently and selectively inhibited by brefeldin A, an ARF-specific disrupting agent (Faundez *et al.*, 1997). Three criteria suggest that ZnT3 is targeted to SV by the AP-3 pathway: ZnT3 interacts with AP-3 through its carboxy-terminal tail in vitro, ZnT3 content in SV and larger brain membranes depends on the presence of functional AP-3, and ZnT3 subcellular distribution and targeting to SLMV are modified by brefeldin A. In contrast, synaptophysin targeting to SLMV is resistant to brefeldin A (Blagoveshchenskaya *et al.*, 1999), and its sorting to brain SV remains unaltered in the absence of functional AP-3, thus suggesting that synaptophysin and ZnT3 preferentially follow distinct intracellular trafficking routes. However, in the absence of AP-3, a fifth of ZnT3 is still able to reach synaptic vesicles, implying that a proportion of ZnT3 can be sorted by an AP-3–independent mechanism. This interpretation is in harmony with the biochemical studies in isolated SV and SLMV, indicating that synaptophysin-rich vesicles do contain ZnT3, although at low levels.

A completely different pharmacological strategy also argues in favor of the hypothesis that, to different extents, SV proteins get sorted to SV by more than one mechanism. Plasma membrane cholesterol depletion either completely or partially inhibits the internalization of several proteins and/or vesicle carriers from the plasma membrane (Rodal *et al.*, 1999; Thiele *et al.*, 2000) without affecting early endosomes (Subtil *et al.*, 1999). In PC12 cells, this treatment blocks the targeting of synaptophysin to SLMV by a 65%, with lesser effects on ClC3, Vglut1, and VAMPII. Surprisingly, intracellular transferrin receptor levels and the ZnT3 content in SLMV are poorly affected by cholesterol depletion, indicating that some endocytic events and also the postendocytic
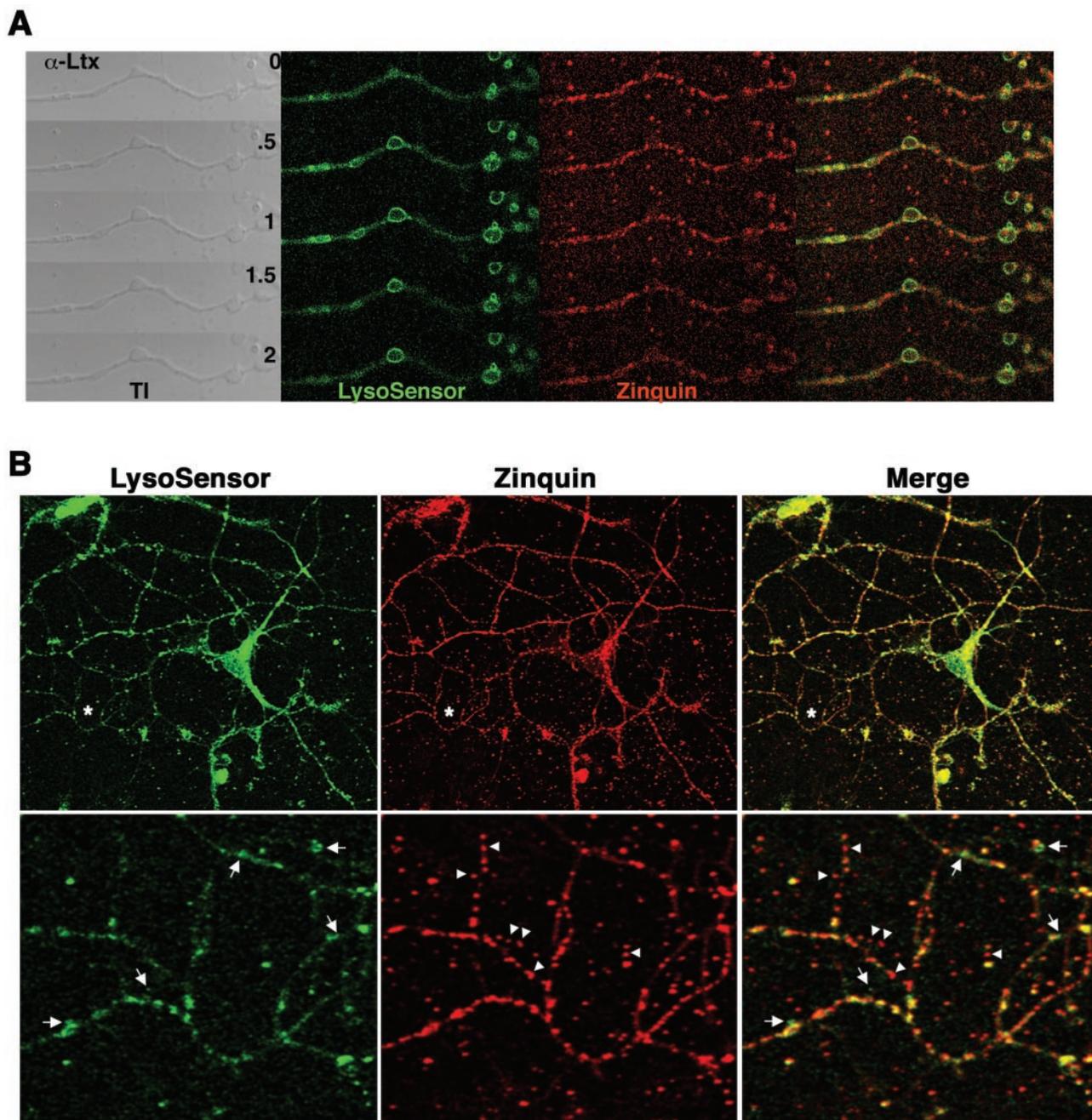
Figure 8. Hippocampal neuron secretory compartments are heterogeneous in composition. (A) Hippocampal neurons were zinc-loaded and double stained with zinquin and LysoSensor DND-189 and the excess of dyes washed away. Neurons were time-lapse imaged and challenged with 10 nM α-latrotoxin at 37°C. LysoSensor DND-189 fluorescence is translocated to the plasma membrane and then decreases, whereas the zinquin signal is progressively reduced over time. The effect of the toxin was monitored in the transmitted image channel through the bouton engorgement. Depicted is one experiment of three performed in duplicate. (B) Hippocampal neurons (14 DIV) were double-labeled as described. Cell were washed and simultaneously imaged in vivo by two-photon microscopy (zinquin) and confocal microscopy (LysoSensor DND-189). Asterisks (top) mark region magnified in the bottom. Boutons and interbouton processes were stained with both dyes; however, zinquin-positive areas were not stained to the same extent with Lysosensor. Arrowheads depict an individual process were boutons positive for zinquin show a wide range of LysoSensor staining. Note the zinquin-positive boutons that do not stain with LysosSensor. Arrows mark LysoSensor-positive puncta that do not stain for zinquin. Similar results were obtained in five independent experiments performed at least in duplicate.

formation of SLMV are insensitive to the plasma membrane cholesterol levels. Despite the fact that ZnT3 targeting to SLMV is insensitive to cholesterol depletion, the trafficking of this protein to SLMV is hindered by brefeldin A. The

different AP-3 binding capabilities of synaptophysin and ZnT3, their differential behavior in the absence of functional AP-3, and the distinct effects of pharmacological agents upon their targeting to SLMV indicate that these proteins are

likely enriched in different vesicle carriers. We have provided supporting evidence for this hypothesis by using immuno-magnetic isolation of PC12 SLMV and rat brain SV. In these experiments, ZnT3 is preferentially targeted to vesicles that contain low levels of synaptophysin. The simplest interpretation of all our results is that these proteins preferentially follow different membrane trafficking pathways to reach distinct SV.

The use of lipophilic dyes, such as FM1-43 and FM2-20, in living cells provides a powerful way to assess different SV pools in individual nerve terminals (Kraszewski *et al.*, 1996; Kuromi and Kidokoro, 1998; Cochilla *et al.*, 1999; Quigley *et al.*, 1999; Rafuse *et al.*, 2000; Richards *et al.*, 2000). Using this model, we designed a vital staining strategy incorporating the zinc-indicator zinquin (Zalewski *et al.*, 1993, 1994; Snitsarev *et al.*, 2001) and the pH-indicator LysoSensor Green DND-189 (Lin *et al.*, 2001). Both dyes possess fluorescent properties that depend on the biochemical environment where they partition. We have taken advantage of the observation that synaptic vesicles loaded in vitro with zinc increase their pH (Goncalves *et al.*, 1999). If in a neuron all SV possess similar zinc and proton transport activities, dual staining with these dyes should not discriminate domains; however, a significant number of boutons that stain positive for zinquin are poorly stained with LysoSensor Green, indicating that within a neuron there exist vesicular compartments that differ in their zinc and proton content. Whether the differences in zinc and proton content are due to different activities of the vacuolar ATPase and ZnT3, to a different vesicle protein composition, or both remains to be resolved. Two potential caveats need to be mentioned in this vital staining procedure. 1) Are the labeled compartments synaptic vesicles? 2) Does zinquin fluorescence report ZnT3 function? In our cultured neurons, both fluorescent signals are mobilized in the presence of α-latrotoxin, arguing in favor of their presence in synaptic vesicles. On the other hand, we estimate that most of the zinquin fluorescence detected by us is due to ZnT3 because ZnT3 $-/-$ mice completely lack ionic zinc in their hippocampus (Cole *et al.*, 1999). However, the contribution of other zinc transporters expressed in brain, although likely to be minor (Huang, 1997; Huang *et al.*, 2002; Kambe *et al.*, 2002), cannot be ruled out yet. Nonetheless, our confocal microscopy immuno-localization studies in hippocampal neurons and the biochemical analysis of brain SV from wild-type and AP-3–deficient mocha brains support the hypothesis that vesicles possess variable stoichiometry of their constituents.

AP-3 $-/-$ brain membranes and synaptic vesicles possess reduced levels of ZnT3 content but not synaptophysin. We believe the decrease is likely mostly synaptic because the majority of the ZnT3 immunoreactivity in brain is synaptic and little is observed in cell bodies (Wenzel *et al.*, 1997; our unpublished observations). In fact, the low levels of ZnT3 immunoreactivity remain in the cell bodies of AP-3 $-/-$ mouse brain neurons (Kantheti *et al.*, 1998, 2003), suggesting that the reduction in the ZnT3 levels is likely a post-Golgi effect. Moreover, whether we analyzed the ZnT3 levels in SV derived from *mocha* or in the AP-3 hypomorph allele *mocha 2J*, we detect a similar reduction (our unpublished observations). These results are striking because in *mocha 2J*, ZnT3 levels are reduced in neocortex but not in hippocampus (Kantheti *et al.*, 2003), suggesting that cells that possess normal ZnT3 levels do not target the transporter to SV. The identification of new SV proteins enriched in AP-3–derived synaptic vesicles will help us to clarify the role that the absence of AP-3 possess on the fate of membrane protein at the synapse or elsewhere in the neuron.

A model compatible with our findings both in PC12 cells as well as wild-type and AP-3–deficient brain is that some synaptic vesicles antigens, such as synaptophysin and ZnT3, can be facultatively sorted to distinct but overlapping vesicle populations. The extent of overlapping is likely determined by the relative proportion of endosomal and plasma membrane routes present in a cell domain (Zakharenko *et al.*, 1999), the developmental status of the cell (Rafuse *et al.*, 2000), the affinities of the synaptic vesicle proteins for different adaptors, the association of several vesicle antigens in complexes with other SV proteins (Bennett *et al.*, 1992), the lipid composition of the membrane (Mitter *et al.*, 2003), and the functional status of the synapse (Heuser and Reese, 1973).

Functional diversity of synapses is a universal feature present not only on different neurons but also in the multiple synapses made by the same neuron (Atwood and Karunanithi, 2002). Both presynaptic and postsynaptic mechanisms contribute to the generation of this functional variety (Craig and Boudin, 2001; Atwood and Karunanithi, 2002). Electrophysiological studies on mossy fiber synapses indicate that the glutamatergic and GABAergic secretory components of a single cell behave as if they were packed in different secretory vesicles (Walker *et al.*, 2001). Our evidence suggests that the functional diversity of synapses could also result from heterogeneity in SV composition dictated by the biogenesis pathway followed. These potential mechanisms could provide a layer of complexity to regulate the quality and quantity of different small molecule mediators into distinct vesicles.

REFERENCES

Atwood, H.L., and Karunanithi, S. (2002). Diversification of synaptic strength: presynaptic elements. Nat. Rev. Neurosci. *3*, 497–516.

Baumert, M., Maycox, P.R., Navone, F., De Camilli, P., and Jahn, R. (1989). Synaptobrevin: an integral membrane protein of 18, 000 daltons present in small synaptic vesicles of rat brain. EMBO J. *8*, 379–384.

Bellocchio, E.E., Reimer, R.J., Fremeau, R.T., Jr., and Edwards, R.H. (2000). Uptake of glutamate into synaptic vesicles by an inorganic phosphate transporter. Science *289*, 957–960.

Bennett, M.K., Calakos, N., Kreiner, T., and Scheller, R.H. (1992). Synaptic vesicle membrane proteins interact to form a multimeric complex. J. Cell Biol. *116*, 761–775.

Blagoveshchenskaya, A.D., Hewitt, E.W., and Cutler, D.F. (1999). A complex web of signal-dependent trafficking underlies the triorganellar distribution of P-selectin in neuroendocrine PC12 cells. J. Cell Biol. *145*, 1419–1433.

Blumstein, J., Faundez, V., Nakatsu, F., Saito, T., Ohno, H., and Kelly, R.B. (2001). The neuronal form of adaptor protein-3 is required for synaptic vesicle formation from endosomes. J. Neurosci. *21*, 8034–8042.

Boehm, M., and Bonifacino, J.S. (2001). Adaptins: the final recount. Mol. Biol. Cell *12*, 2907–2920.

Bonifacino, J.S., and Dell'Angelica, E.C. (1999). Molecular bases for the recognition of tyrosine-based sorting signals. J. Cell Biol. *145*, 923–926.

Bonzelius, F., Herman, G.A., Cardone, M.H., Mostov, K.E., and Kelly, R.B. (1994). The polymeric immunoglobulin receptor accumulates in specialized endosomes but not synaptic vesicles within the neurites of transfected neuroendocrine PC12 cells. J. Cell Biol. *127*, 1603–1616.

Clift-O'Grady, L., Desnos, C., Lichtenstein, Y., Faundez, V., Horng, J.T., and Kelly, R.B. (1998). Reconstitution of synaptic vesicle biogenesis from PC12 cell membranes. Methods *16*, 150–159.

Clift-O'Grady, L., Linstedt, A.D., Lowe, A.W., Grote, E., and Kelly, R.B. (1990). Biogenesis of synaptic vesicle-like structures in a pheochromocytoma cell line PC-12. J. Cell Biol. *110*, 1693–1703.

Cochilla, A.J., Angleson, J.K., and Betz, W.J. (1999). Monitoring secretory membrane with FM1–43 fluorescence. Annu. Rev. Neurosci. *22*, 1–10.

Cole, T.B., Wenzel, H.J., Kafer, K.E., Schwartzkroin, P.A., and Palmiter, R.D. (1999). Elimination of zinc from synaptic vesicles in the intact mouse brain by disruption of the ZnT3 gene. Proc. Natl. Acad. Sci. USA *96*, 1716–1721.

Craig, A.M., and Boudin, H. (2001). Molecular heterogeneity of central synapses: afferent and target regulation. Nat. Neurosci. *4*, 569–578.

Craven, S.E., El-Husseini, A.E., and Bredt, D.S. (1999). Synaptic targeting of the postsynaptic density protein PSD-95 mediated by lipid and protein motifs. Neuron *22*, 497–509.

Daly, C., and Ziff, E.B. (2002). Ca2+-dependent formation of a dynamin-synaptophysin complex: potential role in synaptic vesicle endocytosis. J. Biol. Chem. *277*, 9010–9015.

de Wit, H., Lichtenstein, Y., Geuze, H., Kelly, R.B., van der Sluijs, P., and Klumperman, J. (1999). Synaptic vesicles form by budding from tubular extensions of sorting endosomes in PC12 cells. Mol. Biol. Cell *10*, 4163–4176.

de Wit, H., Lichtenstein, Y., Kelly, R.B., Geuze, H.J., Klumperman, J., and van der Sluijs, P. (2001). Rab4 regulates formation of synaptic-like microvesicles from early endosomes in PC12 cells. Mol. Biol. Cell *12*, 3703–3715.

Dell'Angelica, E.C., Ohno, H., Ooi, C.E., Rabinovich, E., Roche, K.W., and Bonifacino, J.S. (1997). AP-3, an adaptor-like protein complex with ubiquitous expression. EMBO J. *16*, 917–928.

Faundez, V., Horng, J.T., and Kelly, R.B. (1997). ADP ribosylation factor 1 is required for synaptic vesicle budding in PC12 cells. J. Cell Biol. *138*, 505–515.

Faundez, V., Horng, J.T., and Kelly, R.B. (1998). A function for the AP3 coat complex in synaptic vesicle formation from endosomes. Cell *93*, 423–432.

Faundez, V.V., and Kelly, R.B. (2000). The AP-3 complex required for endosomal synaptic vesicle biogenesis is associated with a casein kinase ialpha-like isoform. Mol. Biol. Cell *11*, 2591–2604.

Goncalves, P.P., Meireles, S.M., Neves, P., and Vale, M.G. (1999). Ionic selectivity of the Ca2+/H+ antiport in synaptic vesicles of sheep brain cortex. Brain Res. Mol. Brain Res. *67*, 283–291.

Grote, E., Hao, J.C., Bennett, M.K., and Kelly, R.B. (1995). A targeting signal in VAMP regulating transport to synaptic vesicles. Cell *81*, 581–589.

Herman, G.A., Bonzelius, F., Cieutat, A.M., and Kelly, R.B. (1994). A distinct class of intracellular storage vesicles, identified by expression of the glucose transporter GLUT4. Proc. Natl. Acad. Sci. USA *91*, 12750–12754.

Heuser, J.E., and Reese, T.S. (1973). Evidence for recycling of synaptic vesicle membrane during transmitter release at the frog neuromuscular junction. J. Cell Biol. *57*, 315–344.

Huang, E.P. (1997). Metal ions and synaptic transmission: think zinc. Proc. Natl. Acad. Sci. USA *94*, 13386–13387.

Huang, L., Kirschke, C.P., and Gitschier, J. (2002). Functional characterization of a novel mammalian zinc transporter, ZnT6. J. Biol. Chem. *277*, 26389–26395.

Jarousse, N., and Kelly, R.B. (2001). Endocytotic mechanisms in synapses. Curr. Opin. Cell Biol. *13*, 461–469.

Kambe, T., Narita, H., Yamaguchi-Iwai, Y., Hirose, J., Amano, T., Sugiura, N., Sasaki, R., Mori, K., Iwanaga, T., and Nagao, M. (2002). Cloning and characterization of a novel mammalian zinc transporter, zinc transporter 5, abundantly expressed in pancreatic beta cells. J. Biol. Chem. *277*, 19049–19055.

Kantheti, P., Diaz, M.E., Peden, A.E., Seong, E.E., Dolan, D.F., Robinson, M.S., Noebels, J.L., and Burmeister, M.L. (2003). Genetic and phenotypic analysis of the mouse mutant mh(2J), an Ap3d allele caused by IAP element insertion. Mamm. Genome *14*, 157–167.

Kantheti, P., *et al*. (1998). Mutation in AP-3 delta in the mocha mouse links endosomal transport to storage deficiency in platelets, melanosomes, and synaptic vesicles. Neuron *21*, 111–122.

Kirchhausen, T. (1999). Adaptors for clathrin-mediated traffic. Annu. Rev. Cell Dev. Biol. *15*, 705–732.

Kraszewski, K., Daniell, L., Mundigl, O., and De Camilli, P. (1996). Mobility of synaptic vesicles in nerve endings monitored by recovery from photobleaching of synaptic vesicle-associated fluorescence. J. Neurosci. *16*, 5905–5913.

Kuromi, H., and Kidokoro, Y. (1998). Two distinct pools of synaptic vesicles in single presynaptic boutons in a temperature-sensitive *Drosophila* mutant, shibire. Neuron *20*, 917–925.

Le Bivic, A., Real, F.X., and Rodriguez-Boulan, E. (1989). Vectorial targeting of apical and basolateral plasma membrane proteins in a human adenocarcinoma epithelial cell line. Proc. Natl. Acad. Sci. USA *86*, 9313–9317.

Lichtenstein, Y., Desnos, C., Faundez, V., Kelly, R.B., and Clift-O'Grady, L. (1998). Vesiculation and sorting from PC12-derived endosomes in vitro. Proc. Natl. Acad. Sci. USA *95*, 11223–11228.

Lin, H.J., Herman, P., Kang, J.S., and Lakowicz, J.R. (2001). Fluorescence lifetime characterization of novel low-pH probes. Anal. Biochem. *294*, 118–125.

Linstedt, A.D., and Kelly, R.B. (1991a). Endocytosis of the synaptic vesicle protein, synaptophysin, requires the COOH-terminal tail. J. Physiol. *85*, 90–96.

Linstedt, A.D., and Kelly, R.B. (1991b). Synaptophysin is sorted from endocytotic markers in neuroendocrine PC12 cells but not transfected fibroblasts. Neuron *7*, 309–317.

Mitter, D., Reisinger, C., Hinz, B., Hollmann, S., Yelamanchili, S.V., Treiber-Held, S., Ohm, T.G., Herrmann, A., and Ahnert-Hilger, G. (2003). The synaptophysin/synaptobrevin interaction critically depends on the cholesterol content. J. Neurochem. *84*, 35–42.

Palmiter, R.D., Cole, T.B., Quaife, C.J., and Findley, S.D. (1996). ZnT-3, a putative transporter of zinc into synaptic vesicles. Proc. Natl. Acad. Sci. USA *93*, 14934–14939.

Quigley, P.A., Msghina, M., Govind, C.K., and Atwood, H.L. (1999). Visible evidence for differences in synaptic effectiveness with activity-dependent vesicular uptake and release of FM1-43. J. Neurophysiol. *81*, 356–370.

Rafuse, V.F., Polo-Parada, L., and Landmesser, L.T. (2000). Structural and functional alterations of neuromuscular junctions in NCAM-deficient mice. J. Neurosci. *20*, 6529–6539.

Richards, D.A., Guatimosim, C., and Betz, W.J. (2000). Two endocytic recycling routes selectively fill two vesicle pools in frog motor nerve terminals [In Process Citation]. Neuron *27*, 551–559.

Rodal, S.K., Skretting, G., Garred, O., Vilhardt, F., van Deurs, B., and Sandvig, K. (1999). Extraction of cholesterol with methyl-beta-cyclodextrin perturbs formation of clathrin-coated endocytic vesicles. Mol. Biol. Cell *10*, 961–974.

Roos, J., and Kelly, R.B. (1998). Dap160, a neural-specific Eps15 homology and multiple SH3 domain-containing protein that interacts with *Drosophila* dynamin. J. Biol. Chem. *273*, 19108–19119.

Salem, N., Faundez, V., Horng, J.T., and Kelly, R.B. (1998). A v-SNARE participates in synaptic vesicle formation mediated by the AP3 adaptor complex. Nat. Neurosci. *1*, 551–556.

Schmidt, A., Hannah, M.J., and Huttner, W.B. (1997). Synaptic-like microvesicles of neuroendocrine cells originate from a novel compartment that is continuous with the plasma membrane and devoid of transferrin receptor [published erratum appears in J. Cell Biol. 1997 June 2;137(5):1197]. J. Cell Biol. *137*, 445–458.

Shi, G., Faundez, V., Roos, J., Dell'Angelica, E.C., and Kelly, R.B. (1998). Neuroendocrine synaptic vesicles are formed in vitro by both clathrin-dependent and clathrin-independent pathways. J. Cell Biol. *143*, 947–955.

Snitsarev, V., Budde, T., Stricker, T.P., Cox, J.M., Krupa, D.J., Geng, L., and Kay, A.R. (2001). Fluorescent detection of Zn(2+)-rich vesicles with zinquin: mechanism of action in lipid environments. Biophys. J. *80*, 1538–1546.

Springer, S., Spang, A., and Schekman, R. (1999). A primer on vesicle budding. Cell *97*, 145–148.

Stobrawa, S.M., *et al*. (2001). Disruption of ClC-3, a chloride channel expressed on synaptic vesicles, leads to a loss of the hippocampus. Neuron *29*, 185–196.

Subtil, A., Gaidarov, I., Kobylarz, K., Lampson, M.A., Keen, J.H., and McGraw, T.E. (1999). Acute cholesterol depletion inhibits clathrin-coated pit budding. Proc. Natl. Acad. Sci. USA *96*, 6775–6780.

Takamori, S., Rhee, J.S., Rosenmund, C., and Jahn, R. (2000). Identification of a vesicular glutamate transporter that defines a glutamatergic phenotype in neurons. Nature *407*, 189–194.

Thiele, C., Hannah, M.J., Fahrenholz, F., and Huttner, W.B. (2000). Cholesterol binds to synaptophysin and is required for biogenesis of synaptic vesicles. Nat. Cell Biol. *2*, 42–49.

van de Goor, J., Ramaswami, M., and Kelly, R. (1995). Redistribution of synaptic vesicles and their proteins in temperature-sensitive shibire(ts1) mutant *Drosophila*. Proc. Natl. Acad. Sci. USA *92*, 5739–5743.

Walker, M., Ruiz, A., and Kullmann, D. (2001). Monosynaptic GABAergic signaling from dentate to CA3 with a pharmacological and physiological profile typical of mossy fiber synapses. Neuron *29*, 703–715.

Wei, M.L., Bonzelius, F., Scully, R.M., Kelly, R.B., and Herman, G.A. (1998). GLUT4 and transferrin receptor are differentially sorted along the endocytic pathway in CHO cells. J. Cell Biol. *140*, 565–575.

Wenzel, H.J., Cole, T.B., Born, D.E., Schwartzkroin, P.A., and Palmiter, R.D. (1997). Ultrastructural localization of zinc transporter-3 (ZnT-3) to synaptic vesicle membranes within mossy fiber boutons in the hippocampus of mouse and monkey. Proc. Natl. Acad. Sci. USA *94*, 12676–12681.

Wiedenmann, B., and Franke, W.W. (1985). Identification and localization of synaptophysin, an integral membrane glycoprotein of Mr 38, 000 characteristic of presynaptic vesicles. Cell *41*, 1017–1028.

Wu, X., Zhao, X., Baylor, L., Kaushal, S., Eisenberg, E., and Greene, L.E. (2001). Clathrin exchange during clathrin-mediated endocytosis. J. Cell Biol. *155*, 291–300.

Zakharenko, S., Chang, S., O'Donoghue, M., and Popov, S.V. (1999). Neurotransmitter secretion along growing nerve processes: comparison with synaptic vesicle exocytosis. J. Cell Biol. *144*, 507–518.

Zalewski, P.D., Forbes, I.J., and Betts, W.H. (1993). Correlation of apoptosis with change in intracellular labile Zn(II) using zinquin [(2-methyl-8-p-toluenesulphonamido-6-quinolyloxy)acetic acid], a new specific fluorescent probe for Zn(II). Biochem. J. *296*, 403–408.

Zalewski, P.D., Millard, S.H., Forbes, I.J., Kapaniris, O., Slavotinek, A., Betts, W.H., Ward, A.D., Lincoln, S.F., and Mahadevan, I. (1994). Video image analysis of labile zinc in viable pancreatic islet cells using a specific fluorescent probe for zinc. J. Histochem. Cytochem. *42*, 877–884.

Zhou, Q., Petersen, C.C., and Nicoll, R.A. (2000). Effects of reduced vesicular filling on synaptic transmission in rat hippocampal neurones. J. Physiol. 525, 195–206.